Optical flow analysis reveals that Kinesin-mediated advection impacts on the orientation of microtubules

Maik Drechsler[1,2,6,#], Lukas F. Lang[3,#], Hendrik Dirks[4], Martin Burger[5], Carola-Bibiane Schönlieb[3] and Isabel M. Palacios[1,6]

[1]*School of Biological and Chemical Sciences, Queen Mary University of London, Mile End Road, London E1 4NS, UK and Department of Zoology, University of Cambridge, Cambridge CB2 3EJ, UK*

[2]*Department of Zoology and Developmental Biology, University of Osnabrück, Barbarastraße 11, 49076 Osnabrück, Germany*

[3]*Department of Applied Mathematics and Theoretical Physics, University of Cambridge, Wilberforce Road, Cambridge CB3 0WA, UK*

[4]*Institute for Computational and Applied Mathematics, University of Münster, Einsteinstraße 62, 48149 Münster, Germany*

[5]*Department of Mathematics, Friedrich-Alexander Universität Erlangen-Nürnberg, Cauerstraße 11, 91058 Erlangen, Germany*

[6]*Corresponding authors: drechsler@biologie.uni-osnabrueck.de, i.palacios@qmul.ac.uk tel. +44 (0)20 7882 6909*

[#]equal contribution

Key words: *self-organisation; active processes; optical flow; advection; asymmetries; polarity; cytoskeleton; microtubules; actin; motor proteins; body plan; oogenesis*

ABSTRACT

The polar orientation of microtubule networks is exploited by molecular motors, such as kinesins, to deliver cargoes to specific intracellular destinations, and is thus essential for cell polarity and cell function. Reconstituted *in vitro* systems have largely contributed to the current understanding of the molecular framework, regulating the behaviour of single microtubule filaments. In cells however, microtubules are subjected to a variety of different biomechanical forces that might impact on their orientation and thus on the organisation of the entire network. Here we implement variational optical flow analysis as a new approach to analyse the polarity of microtubule networks *in vivo*, and find that cytoplasmic flows impact on the growth direction of microtubule plus ends in the *Drosophila* oocyte. We provide a thorough characterisation of microtubule behaviour and orientation under different kinesin-dependent cytoplasmic flow conditions, and establish that flows are sufficient and necessary to support the overall organisation of the microtubule cytoskeleton.

Introduction

Eukaryotic life depends on many dynamic processes, including for example cell division, cell migration, and cell polarisation. These processes in turn strongly rely on highly organised microtubule (MT) arrays. All MT networks are polarised, with the minus end of each filament linked to a nucleating centre (MT organising centre or MTOC), and the plus end growing away from these centres. This intrinsic polarity is utilised by specific motor proteins to transport cargo along MTs in a defined direction, and is essential for the function of MT networks, and consequently for the function and polarity of cells.

A number of biophysical studies in reconstituted *in vitro* systems have helped to understand the mechanical properties of MTs, setting the stage to investigate the behaviour of MTs *in vivo*. However, much needs to be learnt about the properties of MTs in their natural intracellular environment. For example, a rather new concept emanating from *in vivo* experiments is that controlling nucleation and the position of minus ends alone is not always sufficient to establish the proper polarity of the network. Thus MT plus ends must be controlled as well in order to allow motor proteins to deliver their cargoes to the correct destination. The plus ends can be regulated at various levels, including dynamic instability, capturing, and direction of growth. Dynamic instability describes a process, in which MT polymerisation is interrupted by a rapid depolymerisation phase, followed by a 'rescue' process[1]. Various MT-associated proteins, such as molecular motors and MT plus end-tracking proteins (+TIPs), are known to regulate dynamic instability[2]. Furthermore, MT plus ends can also be stabilised by cortical capture, also involving +TIPs and other molecules such as the Dynein/Dynactin complex[3] (and as reviewed in[2]). However, very little is known about how the direction of growth of plus ends, and therefore the orientation of MTs, is controlled in cells. In axons, adenomatous polyposis coli (APC) regulates MT looping, probably by controlling plus end direction[4], while Fidgetin-like1, a MT-associated ATPase, controls both dynamics and plus ends direction[5]. MT bending also impacts on the direction of plus tip growth, as the MT tip has been seen to rotate due to local bend formation[6]. Furthermore, +TIPs that contain actin-binding domains can influence MT growth direction by guiding dynamic plus ends along actin bundles[7,8].

A striking example of MT-dependent cell polarisation takes place in the oocyte of *Drosophila melanogaster*, where the MT cytoskeleton directs the asymmetric localisation of body plan determinants. For example, the plus end motor Kinesin-1 (Kin from here on) is essential for the localisation of *oskar* mRNA to the posterior pole of the mid-oogenesis stage 9 (st9) oocyte, an essential step in the establishment of the anterior-posterior (A-P) axis and the formation of the germ cells of the embryo. The st9 oocyte is roughly hemispherical, extending approximately 80-100µm along the A-P axis. MTs are nucleated from the antero-lateral cortex in a gradient of diminishing abundance toward the posterior pole, where nucleation is absent, while the growing plus ends exhibit a weak global posterior orientation bias[9-11]. In the oocyte, Kin is also responsible for inducing the advective motion of cytoplasmic content, called cytoplasmic streaming (or cytoplasmic flows)[12],

which mixes the cytoplasm of the large oocyte[13], and aids the localisation of developmental determinants and mitochondria[14-16].

So far it is debatable how flows are actually induced, whether by viscous drag of translocating Kin molecules[17], sliding of microtubules[18], or both. However, it has been shown that they have an impact on the organisation of the cytoplasm. Recently we found that Kin-mediated cytoplasmic flows constitute a key force driving the ballistic, persistent motion of cytoplasmic vesicles as well as actin filaments in st9 oocytes[19]. These observations prompted us to study the *in vivo* behaviour of MTs under different flow conditions, and to address the question of how advection impacts on the organisation of the MT network in the oocyte.

In order to assess the global MT orientation, and to investigate the growth direction of MT plus ends, we used EB1::GFP (EB1 from here on) to follow MT growth *in vivo*. EB1 exclusively decorates the growing plus end of MTs, resulting in dynamic 'comets' moving through the cytoplasm[20]. Analysing the dynamic behaviour of MTs and their orientation in complex MT networks has proven technically challenging, and requires suitable imaging and image analysis tools. Especially for the *Drosophila* oocyte, we found the published methods too demanding on the imaging level, requiring state of the art wide-field deconvolution microscopy and rather elaborate image processing[9]. Consequently, we found it to be an unfeasible approach for the various experimental conditions that our study required. Therefore, we developed a new image analysis pipeline that allows an efficient and reliable characterisation of direction and distribution of the growth of EB1-labelled 'comets' *in vivo*.

In the present study, we demonstrate a strategy to assess the architecture of the dense MT network found in *Drosophila* oocytes from confocal image series by an optical flow-based motion estimation (OF) approach. In general OF allows to estimate the apparent motion of intensities, like fluorescence signals, from a sequence of images[21]. Variational OF methods, furthermore constitute a well-established and powerful framework for reliable dense motion estimation, omitting elaborate segmentation or tracking of the studied structures. Importantly, OF methods have been shown to outperform popular methods, such as particle image velocimetry (PIV), for motion analysis, resulting in higher accuracy and efficiency in certain settings and, in particular, in the presence of noise[22,23]. While variational OF methods have been used predominantly to investigate the dynamics of entire cells[24-31], recent works focused on their application to study intracellular motility as well[22,32-35]. The high noise level, poor contrast, and the relatively small size of the EB1 comets, constituted the main challenges in the analysis of our data. Consequently, classical methods (such as particle tracking or PIV) either failed or struggled to extract reliable results from confocal EB1 images.

Here, we demonstrate a two-step image analysis approach that is based on variational OF and is able to estimate approximate velocities (speed and direction) of EB1 comets in confocal image sequences in a reliable and efficient manner. This allowed us for the first time to investigate the organisation of the MT cytoskeleton along the entire A-P axis of the *Drosophila* oocyte, and revealed that cytoplasmic flows are sufficient and necessary to regulate the polarity of this MT network.

RESULTS

Cytoplasmic flows are sufficient to alter the bulk movement, bundling and length of MTs

In st9 oocytes, the velocities of cytoplasmic flows directly correlate with Kin activity, while the pattern and topology of these flows are tightly linked to the architecture of the underlying MT network[13]. We recently found that cytoplasmic flows are a major force, driving the persistent motion - and supporting the active diffusion - of cytoplasmic vesicles and actin filaments[19]. These findings prompted us to investigate the impact of flows and advection on the behaviour of MTs. We first imaged the MT-associated protein Jupiter::GFP (Jup from here on)[36] in st9 oocytes by confocal microscopy and monitored the dynamic behaviour of MTs over time (Figure 1a). The acquired time-lapse sequences showed that MTs undergo a significant bulk movement and 'flow' through the oocyte (Supplementary Movie 1). Kymographs along the lateral axis of the cell also revealed that MTs are subjected to dynamic bending, and thereby change their spatial orientation over time (Figure 1a').

Previously, it has been shown that artificial fast fluid flows affect the dynamic behaviour of MTs in the oocyte[37]. To investigate how changing the regime of flows affects MT behaviour in more detail, we monitored Jup-labelled MTs in oocytes lacking the formin Cappuccino (Capu). Capu constitutes an actin nucleator, necessary for the formation of a cytoplasmic actin mesh. This specialised actin network traverses the oocyte and counteracts Kin-induced cytoplasmic flows. Thus, oocytes without Capu lack the actin mesh and display faster streaming[38,39]. Consistently, we observed that MTs in *capu* mutant oocytes appear as thick bundles, that dramatically bend and buckle. These bundles are likely a result of an increase in MT density by 'clustering' in certain areas of the cell (Figure 1c,c', Supplementary Movie 1). However, while previously described as subcortical arrays[37], our data demonstrates that in *capu* mutants MTs bundle, even when they are not in immediate proximity to the cell cortex. Finally, the observed MT bundles appear longer compared to control cells, and frequently extend far into the posterior regions of the oocyte (red arrow in Figure 1c). Our results suggest that changing the regime of cytoplasmic flows impacts on the bulk movement, the bundling state, and the length of MTs in the oocyte.

Quantification of MT plus-tip directionality by optical flow analysis

In addition to exhibiting fast cytoplasmic flows, *capu* mutant oocytes also fail to localise posterior cargo such as *oskar* mRNA or the *oskar* mRNA-binding protein Staufen (Figure 1d)[38]. Since cytoplasmic flows obviously affect the bulk movement of MTs, we therefore wondered whether they are also sufficient to alter the spatial orientation of single MT filaments within a cell, which might contribute to the observed cargo localisation defects. In other words, are cytoplasmic flows necessary to maintain the correct polarity of the MT network in wild-type oocytes? To address this question, we used oocytes expressing EB1 (Figure 2a,d and Supplementary Methods). EB1 constitutes a versatile marker for growing plus-tips and has been used in fly oocytes before[3,9]. In these previous studies, widefield deconvolution microscopy was used to image EB1 dynamics in specific areas of the oocyte. However, widefield microscopy has a limited focus depth and works

best on thin samples. Thus widefield microscopy only allows to image EB1 dynamics close to the cortex in *Drosophila* oocytes. We implemented a strategy that combines conventional confocal microscopy, which is widely available and allows to image deeper into the oocyte, with image analysis by variational OF.

OF-based motion estimation relies on the assumption that particles approximately maintain their pixel intensity as they move. As this is formulated on a per-pixel basis, this method allows to infer a displacement vector for each pixel and does not require sophisticated tracking of individual particles (Figure 2b). Since EB1 dynamics demand imaging at a reasonably high frame rate, the confocal raw data exhibits a considerable high noise contamination (Figure 2d). Due to this high noise level, preceding denoising of the image data was required before applying the motion estimation. We found that total variation-based[40] image denoising with additional temporal regularisation was sufficient to obtain a significant improvement of the signal-to-noise ratio and of the visibility of EB1 comets (Figure 2d,e, Supplementary Methods, Supplementary Figures 1-3 and Supplementary Movie 2).

The improved image sequences were then used as input to the second step, in which displacement vector fields were computed with a variational OF method (Supplementary Figure 4). After accounting for the pixel size and the time interval between consecutive frames, these displacements can be regarded as approximate velocities of fluorescence signals and of thus EB1 comets (see Figure 2f-h). A typical image sequence with 100 frames and a pixel resolution of 512 x 256 pixels results in a total number of approximately 13 million computed velocity vectors that require appropriate interpretation. The computation time for processing one typical sequence amounted to less than 25 minutes on average.

We visualised the estimated velocity fields with the help of a standard colour-coding[41]. The velocity vector at each pixel and at a certain frame is represented by a colour that is determined by the direction of the signal's movement (see the colour-coding at the boundary of the images in Figure 2f-h). The plotted colour's intensity is determined by the relative speed of the movement. For our statistical analyses, we considered only velocities of pixels located within a hand-drawn segmentation mask that outlines the oocyte in each sequence (Figures 2h). These velocities can then be represented in polar coordinates, resulting in angles and speeds. For each image sequence, we visualised the distribution of angles in a rose diagram (or angular histogram) in different colours (Figure 2j), and the distribution of angles of multiple sequences in an aggregated way (Figure 2k). First, we used OF to describe MT orientation in control oocytes (Figure 2i-m, Supplementary Figure 5). Since all cells were orientated in the same way during imaging, the angles given in the rose diagram reflect the growth direction of EB1 comets within a cell (with 0° corresponding to posterior and 180° corresponding to anterior). For a quantitative description of MT orientation, we determined the mean angular direction of EB1 signals (θ_{avg}, considering all recorded cells, Figure 2l, Table 1) and the frequency of signals directed towards the anterior (90° to 270°) or the posterior (270° to 90°) (Figure 2l). As a descriptor of how focused MTs grow towards the posterior tip of the cell, we also

182 determined the relative frequency of posterior growing EB1 signals (270° to 90°) that fall within an
183 arbitrarily defined circular sector of 60° (from 330° to 30°, called 'posterior tip', Figure 2c). For control
184 cells, we found that all growing MTs exhibit a global posterior orientation bias, with 66% of all comets
185 growing towards the posterior of the cell (Figure 2l), and 40% of those exhibiting a posterior tip
186 orientation (Figure 2m). These findings are in good agreement with previous reports of directional
187 MT bias in the oocyte[9].

188 In order to validate our two-step variational OF-based approach, we analysed EB1 comets in
189 posterior cells of the follicular epithelium that surrounds the egg chamber (Supplementary Figures 6
190 and 7). Compared to the oocyte, MT organisation in follicle cells is less complex, and MT growth is
191 known to be oriented predominantly outwards (towards basal) in a radial direction (Supplementary
192 Movie 3). Importantly, OF analysis captures the directionality of MTs in the follicle cells accurately,
193 proving the suitability of the approach to estimate MT orientation in cells. Furthermore, we analysed
194 oocytes harbouring a mutation in *gurken (grk)*, which exhibit polarity defects[42,43] as well as mis-
195 oriented MT arrays[44]. As reported before, *grk* mutant oocytes fail to localise the nucleus and our OF
196 analysis was able to detect an aberrant MT organisation (Supplementary Movie 4 and
197 Supplementary Figure 6). EB1 signals showed a variable orientation from cell-to-cell, with an
198 average posterior bias stronger than that found in control cells (Table 1). However, further analyses
199 will be needed to fully understand the aberrant MT orientation in *grk* mutant cells. Nevertheless,
200 taken together we could show that variational OF-based motion estimation provides a powerful and
201 reliable tool to determine the global orientation of MT arrays and to detect alterations in those
202 cytoskeletal networks from confocal image sequences.
203
204 **Cytoplasmic flows are sufficient to alter MT orientation in the oocyte**
205 In c*apu* mutant oocytes, MTs display a higher degree of clustering, which may reflect a higher degree
206 of bundling (Figure 1c). We used OF analysis to investigate whether the observed changes in MT
207 bulk behaviour also affect the orientation of single filaments, and therefore the overall polarity of the
208 MT network. We quantified the directionality of EB1 signals in *capu* mutant cells and observed
209 substantial alterations (Figure 2n-r). Compared to controls, *capu* mutants exhibit a more stringent
210 orientation of MT plus-tips, in which large amounts of comets were in close proximity to each other
211 and growing in the same direction (Figure 2n and Supplementary Movie 5). From this we concluded
212 that fast flows are sufficient to induce arrays of parallel filaments that grow in the same direction,
213 and this finding strongly supports the observation that faster flows cause increased bundling of MTs
214 (Figure 1). Consequently, the orientation of clustered MTs, and thus the direction of EB1 comets,
215 showed a large variability in *capu* mutant cells (Figure 2o,p). However, the global posterior EB1
216 orientation bias was only mildly decreased in *capu* mutants (Figure 2q vs. Figure 2l), indicating that
217 this bias is primarily induced by other processes, like asymmetric nucleation and anchoring or the
218 overall geometry of the cell. Nevertheless, due to the higher degree of variability, posterior-directed
219 MTs grow less focused in *capu* mutants, with only 25% of EB1 signals directed towards the posterior

tip (Figure 2r vs. Figure 2m). Together these results demonstrate that cytoplasmic flows need to be in the right regime for MTs to maintain their proper organisation, and that faster advective motion is sufficient to change the state of bundling, focusing, and the orientation of MT growth.

Cytoplasmic flows are necessary for MTs to display a wild-type organisation and correct polar growth

Our data demonstrate that faster cytoplasmic flows affect the spatial orientation of MTs in the oocyte. Thus, we wondered whether flows might actually be necessary to sustain a proper organisation of the MT network. To address this question, we first analysed the motion of Jup-labelled MTs in oocytes lacking *kinesin heavy chain* (*khc*). The loss of the motor subunit of Kin (*khc*^{27}, from hereon called *khc*^{null}) results in a complete absence of cargo transport towards the posterior pole and a lack of cytoplasmic flows (Figure 3a and Supplementary Figure 9)[12,45]. Compared to control cells, MTs in *khc*^{null} mutant oocytes display very little overall motion and appear rather stiff and immobile (Figure 3f,d and Supplementary Movie 6).

However, oocytes without Kin do not only lack cytoplasmic flows and transport to the posterior, but also display an abnormal actin mesh (Supplementary Figure 8)[19]. To test, whether the altered bulk behaviour of MTs is due to the lack of flows or other aberrations linked to a complete loss of Kin, we monitored MTs in oocytes that carry distinct mutations in the Kin motor domain, resulting in a slower motor (two mutant alleles known as *khc*^{23} and *khc*^{17}, hereafter summarised as *khc*^{slow})[46]. St9 *khc*^{slow} oocytes display a normal cytoplasmic actin mesh (Supplementary Figure 8) and are able to transport a considerable amount of cargo towards the posterior (Figure 3b,c)[47,48]. Importantly, and as in *khc*^{null} cells, they lack any cytoplasmic flows, allowing us to study the impact of advection in the presence of transport (Supplementary Figure 9)[48]. MTs in *khc*^{slow} oocytes display the same immobile behaviour, similar to cells lacking the motor entirely (Supplementary Movie 6). They also appear rather stiff and no motion could be detected in kymographs (Figure 3e,f). These observations strongly indicate that the altered behaviour of MTs in oocytes without Kin is indeed due to a lack of cytoplasmic flows. Thus, cytoplasmic advection is necessary for MTs to display a dynamic wild-type behaviour.

We next analysed EB1 directionality in *khc*^{slow} oocytes (Figure 3g-k). As in control cells, we observed dynamic EB1 comets throughout the cytoplasm (Supplementary Movie 7). However, in stark contrast, the distribution of orientation angles displayed a more focussed bias towards the posterior of the cell (Figure 3i vs. Figure 2k). Consequently, *khc*^{slow} mutant oocytes display an increased posterior plus-tip bias, with 75% of EB1 signals directed towards posterior, compared to 66% in control cells (Figure 3j vs. Figure 2l and Table 1). Furthermore, 54% of these posterior-directed EB1 signals displayed a posterior tip orientation, as compared to 40% in controls (Figure 3k vs. Figure 2m and Table 1). These findings indicate that the orientation of the growing MT plus ends in st9 oocytes does not only depend on nucleation or anchoring of minus ends, but also on the presence

of well-regulated cytoplasmic flows. In other words, flows are necessary for MTs to display a correct polar growth.

Surprisingly, we found that the complete lack of Kin did not result in major changes of the global average MT orientation (Supplementary Movie 7). Unlike *khc*^{slow} oocytes, *khc*^{null} cells display a mean angular direction, posterior orientation bias and plus-tip growth towards the posterior tip that is similar to that of controls (Figure 3l-p, Table 1). This suggests that in the complete absence of Kin activity - and thus in the absence of cargo translocation - flows are not necessary for the correct polarisation of the MT network. While the precise molecular mechanism needs to be investigated in more detail, our data indicate that, in the presence of Kin-mediated transport, cytoplasmic flows are necessary for the wild-type organisation of MTs. It is relevant to point out that the Kin-dependent asymmetric accumulation of Oskar and Dynactin to the posterior pole, contributes to the regulation of MT growth in the posterior region of the oocyte[3,49], and this transport process might be causative for the observed differences in MT polarity between the *khc*^{slow} and the *khc*^{null} oocytes.

To further investigate the impact of cytoplasmic flows and Kin activity on MT orientation, we analysed the regional organisation of the MT network along the A-P axis in control, *khc*^{null}, and *khc*^{slow} oocytes. We divided each oocyte into an anterior and a posterior region (Figure 4a), and analysed EB1 directionality in each of these two regions (Table 1). As previously shown, in control cells the posterior EB1 bias increases along the A-P axis of the oocyte (Figure 4b-d)[9]. In the anterior region, we found 62% of signals directed towards posterior (Figure 4c), while this bias was increased to 74% in the posterior region (Figure 4d). Interestingly, the percentage of signals pointing towards the 'posterior tip' (as defined in Figure 2c) remained rather constant along the A-P axis (40% vs. 41%, Figure 4c,d and Table 1). As already demonstrated for the global posterior EB1 bias (Figure 4b), *khc*^{slow} oocytes showed a dramatic change along the entire A-P axis, with a 74%, posterior bias in the anterior region (Figure 4e vs. Figure 4c) and an even further increased 81% posterior bias in the posterior region (Figure 4f vs. Figure 4d). Additionally, the ratio of signals directed towards the 'posterior tip' in both, anterior and posterior regions of the cell, was substantially increased (Figure 4e,f and Table 1). This clearly demonstrates that slower Kin-mediated transport, and thus the lack of flows, cause a stronger polarisation of the entire MT network towards posterior. While the lack of Kin (*khc*^{null}) seemed to cause only minor defects in the global organisation of the MT cytoskeleton, the regional analysis of EB1 directionality revealed substantial differences to both controls and *khc*^{slow} oocytes. In the anterior region of *khc*^{null} cells, we detected an unexpected drop of the posterior bias to only 56% - compared to 66% in controls -, which indicates that the complete lack of Kin-mediated transport along microtubules does indeed affect MT network organisation. Furthermore, we observed a less focused growth of plus-tips towards posterior (Figure 4g vs. Figures 4c,e). It needs to be mentioned here, that in contrast to *khc*^{slow} cells, oocytes lacking Kin fail to localise their nucleus, which is known to be associated with MT minus ends[50]. Therefore, the observed MT behaviour in *khc*^{null} cells might reflect the mis-localisation of a certain subset of MTOCs in the cell. Contrary to the anterior region, in the posterior region of *khc*^{null} oocytes the posterior bias of EB1

signals was found to be nearly unchanged, with 72% of posterior-directed signals in the mutant and 74% in controls. Remarkably however, MTs in the posterior region of *khc*^{null} cells displayed a more focused growth towards the posterior tip, similar to the slow Kin cells (Figure 4h vs. Figures 4d,f and Table 1).

Taken together, the data allows us to make certain interpretations about the relationship of Kin-activity, cytoplasmic flows, and the organisation of the MT cytoskeleton. Firstly, cytoplasmic flows are sufficient to regulate MT orientation and need to be in a defined regime to ensure proper MT polarisation. Secondly, in the presence of Kin-mediated transport, cytoplasmic flows are necessary to organise the correct posterior orientation bias and plus-tip focusing towards the posterior along the entire A-P axis. And thirdly, together with cytoplasmic flows, other Kin-mediated processes, such as cargo transport to the posterior or nucleus anchoring, affect the organisation of the MT network, supporting published work[3,49].

Reconstitution of cytoplasmic flows in *khc*^{slow} oocytes rescues MT orientation

Our data suggests that Kin-mediated cytoplasmic flows are necessary for the MT network to completely adopt its wild-type polarisation. However, since cargo transport is slightly affected in *khc*^{slow} oocytes, we cannot rule out that mild transport defects also contribute to the aberrant MT orientation detected in those cells. Similarly, *capu* mutant oocytes fail to localise posterior cargo, although, it is unclear if this is solely due to faster streaming, and thus the misorientation of MTs, or whether this reflects other functions of the actin mesh or *capu*[51]. Previously, it was shown that cargo localisation defects in *capu* mutants can be rescued by introducing a *khc*^{slow} mutation. It has also been suggested that fast flows in *capu* mutants are slowed down again by *khc*^{slow}, but this assumption was never tested directly[38].

To address this question, we generated a double mutant stock by meiotic recombination of the alleles *capu*^{EY12344} and *khc*^{17}. First, we investigated posterior cargo localisation in fixed cells. As expected, ~85% (n=20) of *capu,khc*^{slow}/+ cells (which are essentially *capu* mutant cells) failed to correctly localise Staufen to the posterior pole of the cell (Figure 5a). Although a weak crescent could usually be detected, most Staufen protein localised to cytoplasmic clouds in the middle of the cells (Figure 5a vs. Figure 1f). In comparison, ~72% (n=25) of *capu,khc*^{slow} double mutant cells localised Staufen into a posterior crescent. However, the majority of those cells (n=11/18) also showed Staufen accumulation in posterior dots, a phenotype that is usually associated with the *khc*^{slow} alleles (Figure 5b vs. Figure 3b,c). These data confirmed that the generated double mutant is comparable to the previously reported allele[38], and that slow Kin is sufficient to rescue the major cargo localisation defects seen in *capu* mutants. Conversely, since cargo transport was not rescued to wild-type levels, and found to be similar to that observed in *khc*^{slow} oocytes[47], it is clear that the decreased cargo transport efficiency of slow Kin cannot be rescued by re-introducing cytoplasmic flows by the lack of *capu*. However, it is still unclear whether this is still due to a reduced translocation speed of slow Kin, or to a defect in cargo anchoring in *capu* mutant cells[51].

Next we tested whether fast cytoplasmic flows in *capu* mutants are indeed rescued in *capu,khc^{slow}* oocytes. As expected, and similar to *capu* single mutants, *capu,khc^{slow}*/+ cells displayed fast streaming and MTs that strongly clustered or bundled in the anterior part of the cell (Figure 5c, Supplementary Movie 8). In contrast, cytoplasmic flows in *capu,khc^{slow}* double mutant cells were slowed down again and appeared similar to those observed in control cells (Supplementary Figure 9). Most importantly, and as suggested before[38], the bulk movement of MTs in *capu,khc^{slow}* double mutants also resembled that of control cells, strongly supporting that cytoplasmic flows are a major factor contributing to normal MT bulk movement (Figure 5d vs. Figure 1a and Supplementary Movie 8).

To finally test whether the re-establishment of cytoplasmic flows in a *khc^{slow}* background (or the reduction of flow speeds in *capu* background) also rescues MT orientation, we analysed EB1 directionality in *capu,khc^{slow}*/+ (Figure 5e-i) and *capu,khc^{slow}* double mutant oocytes (Figure 5j-n and Supplementary Movie 9). As demonstrated for *capu* single mutants, EB1 comets in *capu,khc^{slow}*/+ oocytes exhibited an increased parallel motion (Supplementary Movie 9). Similar to *capu* single mutants, the posterior bias of EB1 comets displayed a large cell-to-cell variability (Figure 5f,g) and was on average slightly reduced, with 61% of signals pointing towards posterior in *capu,khc^{slow}*/+ cells, compared to 66% in controls (Figure 5h vs. Figure 2l). Furthermore, the fraction of signals pointing towards the posterior tip was found reduced to 34%, as compared to 40% in control cells (Figure 5i and Table 1). These values are similar to what we observed in *capu* mutants (Figure 2n-r), suggesting that the heterozygous presence of a *khc^{slow}* mutant chromosome does not substantially affect the *capu* mutant phenotype. Conversely, EB1 comets in *capu,khc^{slow}* double mutant cells displayed a less clustered motion (Figure 5j and Supplementary Movie 9) and a posterior orientation bias comparable to that of control cells (66% posterior bias Figure 5m vs. Figure 2l and Table 1). Finally, also the fraction of EB1 signals pointing towards the 'posterior tip' was found to be similar in *capu,khc^{slow}* double mutant cells (39%) and controls (40%) (Figure 5n vs. Figure 2m and Table 1), further strengthening the idea that cytoplasmic flows constitute a substantial contributor to a correct MT organisation in the oocyte.

In summary, our results demonstrate that in the absence of *capu* and the actin mesh, *khc^{slow}* is sufficient to restore the correct regime of cytoplasmic flows, resulting in a correct polarisation and organisation of the MT cytoskeleton. Therefore, it seems that the actin mesh is absolutely essential in oocytes that exhibit normal Kin-mediated transport, in order to ensure the proper regulation of cytoplasmic flows, which in turn is an important contributor to the observed MT orientation. However, our analysis in the double mutant also suggests that the actin mesh is not absolutely essential for correct orientation of MT plus ends, indicating that plus-end guiding mechanisms as observed in other cells types[52] might only play a minor role in the oocyte.

DISCUSSION

Here we have developed a novel methodology for the reliable and efficient quantitative description of growth directionality of EB1 comets from confocal image sequences. Our two-step image analysis approach is based on a rigorous computational framework and allows to infer approximate velocities (direction and speed) of EB1 comets. Most importantly, the methodology does not require demanding imaging techniques or computing hardware. The use of a highly efficient iterative optimisation algorithm enabled us to analyse entire image sequences at once, as compared to a frame-by-frame analysis. In comparison to existing techniques, such as particle tracking or PIV, OF allows us to perform robust motion estimation on pixel level in challenging circumstances, such as low signal-to-noise ratios and small particle sizes. Moreover, the image analysis depends only on few parameters that can be easily adjusted. Mainly due to its large size (80-100 µm along the A-P axis) and the fact that MT minus ends are nucleated and anchored along the antero-lateral membranes of the cell, the *Drosophila* st9 oocyte is arguably one of the most challenging *in vivo* systems in which to analyse the dynamic behaviour of growing MT plus ends. The use of confocal microscopy, together with the above-mentioned computational tools, allowed us for the first time to quantify growth directionality of plus ends within a 2D focal plane along the entire oocyte. However, two limitations of the developed methodology need to be pointed out. Firstly, due to the use of a variational framework for the image analysis, both the denoised sequences and the estimated velocities exhibit a loss of contrast, leading to underestimated speeds of EB1 comets. This is particularly due to the temporal regularisation required in both steps to overcome the above-mentioned challenges. Moreover, the small size of EB1 comets and the high noise level proved the application of techniques that are typically used to estimate large displacements, such as coarse-to-fine warping-based OF[53], unfeasible. Secondly, our statistical analyses of growth directions of EB1 comets are based on velocities computed for all pixels within each segmented oocyte. We are aware that not every image pixel portrays exactly one EB1 comet. In summary, the results however demonstrate that our approach will be able to identify plus end growth directionality in most, if not all, cell types and thus constitutes an efficient and reliable analytical framework for MT polarity studies.

Together with others, the present study supports the picture of a complex mechanical and/or biochemical relationship between motion of cytoplasmic components (whether by flows or by transport), cytoplasmic F-actin and MTs in the *Drosophila* oocyte. This holds true for our model system, but is likely transferable to many other cell types. Kin-mediated cargo transport through a highly viscous medium such as the cytoplasm inevitably induces bulk motion of such medium, which will cause lateral displacement forces on MTs and thus induces a feed-back on their orientation. As a consequence, cytoplasmic flows need to be kept at a lower speed and at a biased random pattern in order for the MT network to properly polarise. In the absence of the actin mesh (as in *capu* mutants), there is an increased persistence and speed of flows, resulting in parallel alignment and possibly bundling of MTs, as well as strong defects on MT orientation. The actin mesh - which itself

406 requires Kin activity for its proper organisation[19] - is required for the maintenance of this correct
407 regime of flows.

408 However, it is still unknown how the actin mesh slows down Kin-dependent cytoplasmic flows or how
409 it might affect MT organisation. It has been proposed that the presence of a viscoelastic actin network
410 can increase the effective viscosity of the cytoplasm, and counteract the viscous drag of cargo
411 transport by Kin[54]. Furthermore, in *in vitro* systems, actin-microtubule crosslinking proteins have
412 been demonstrated to allow a potent crosstalk between both filament species, and thus have
413 proposed to coordinate cytoskeletal organisation. However, our data from *capu,khc*^{slow} double
414 mutant oocytes, which do not form an actin mesh, suggest that the mesh is not absolutely essential
415 to allow a correct MT orientation. In this 'artificial' mutant situation, the correct regime of flows seems
416 sufficient to allow proper MT network organisation. This is supported by published work showing that
417 the actin mesh is not altered in colchicine treated oocytes, making a direct crosslinking mechanism
418 between MTs and actin filaments unlikely[38]. Together this shows that in our system, the presence of
419 an F-actin mesh, surrounding MTs, is not absolutely essential to polarise the network. However,
420 other dynamic MT behaviours, such as bending and undulation of single filaments might still be
421 affected, as shown in other as systems[55-58].

422 Lastly, it is reasonable to suspect the actin mesh to regulate the activity of Kin more directly, for
423 example by tethering it to its filaments (directly or indirectly through cargo). Such model is supported
424 by our finding that Kin becomes efficiently recruited to MTs when the mesh is absent (Supplementary
425 Movie 10 and Figure 6). We expressed a KHC::GFP fusion protein (amino acids 1-700) in the female
426 germline, which localises to a posterior cloud and is thought not to interact with any cargo (Figure
427 6)[50]. We found that in control oocytes, this protein only weakly co-localises with MTs, both in fixed
428 and living samples. Upon loss of *capu* however, the fusion protein strongly decorated MTs in the
429 entire cell, suggesting that the actin mesh directly alters the ability of Kin to bind MTs (Figure 6 and
430 Supplementary Movie 10). While these observations are preliminary, they could explain how the
431 mesh regulates cytoplasmic flows in the first place, but also the higher degree of MT bundling in fast
432 flowing oocytes by an effective crosslinking of adjacent filaments by the higher amount of recruited
433 Kin[18].

434 Our data establish cytoplasmic flows in st9 oocytes as a contributing factor for the correct
435 organisation of the MT cytoskeleton. Previous studies suggested that the pattern of nucleation and
436 minus end anchoring along the cortex are sufficient to organise the MT network and to allow correct
437 cargo transport to define the A-P axis of the animal. Consequently, mutant oocytes harbouring
438 defects in nucleation and/or anchoring of minus ends display polarity defects[10,11]. Furthermore,
439 mathematical modelling suggested that cytoplasmic flows at mid-oogenesis are negligible to explain
440 the correct localisation of posterior cargoes like *oskar* mRNA[59]. However, our analysis now
441 demonstrates that dynamic bending of MT filaments in the oocyte takes place, and is mostly driven
442 by cytoplasmic flows. Since we also find that these flows are involved in the orientation of MTs plus

ends, we can conclude that the localisation of the minus ends alone is not enough to define the precise organisation of the network. This was most obvious in *khc*^{slow} oocytes, which in our hands lack cytoplasmic flows entirely, and displayed an increased posterior orientation bias (Figure 3). The advantage of analysing slow Kin mutants is that other Kin-dependent processes, like cargo transport and formation of the actin mesh do take place[19,60]. Despite showing only mild defects in the distribution of developmental determinants, *khc*^{slow} mutant oocytes frequently fail to give rise to a healthy offspring, suggesting that oocyte polarisation is affected[61]. Consistently, we found an increased posterior bias of EB1 signals in *khc*^{slow} mutant oocytes, strongly suggesting that the lack of cytoplasmic flows was causative for this observation.

If and how a stronger posterior polarisation of the MT network may affect cargo delivery to the posterior is unknown. Tracking *oskar* particles in *khc*^{slow} oocytes did not reveal a stronger orientation bias of cargo movement[49]. However, it is unclear whether trajectories of *oskar* transport always reflect the organisation of the underlying MT network, and whether all MTs would be equally used by slow Kin motor/cargo complexes. In mammalian cells, Kin preferentially moves along stable, post-translationally modified MTs[62]. Compared to other cells, MTs in the oocyte are very sensitive against colchicine treatment and appear heavily tyrosinated, a marker of unstable MT filaments[63].

In the absence of Kin-mediated cargo transport (*khc*^{null}), cytoplasmic flows are dispensable for the global posterior MT bias. When analysed only in the posterior region of the oocyte, *khc*^{null} cells did exhibit a weakly increased posterior bias (Figure 4h), which was not as strong as observed in *khc*^{slow} cells (Figure 4f). Besides developmental determinants, Kin also transports the dynein/dynactin motor complex towards the plus end of MTs, which causes a stabilisation of MT growth and consequently amplifies the posterior orientation bias. The lack of Dynactin transport towards the plus end in *khc*^{null} oocytes could therefore contribute to the weaker effects seen on the posterior EB1 bias in these mutants (Figure 4).

In summary, the combination of various forces produced within living cells demands a complex set of biochemical and biomechanical regulatory mechanisms for cytoskeletal networks to organise correctly. Consequently, this calls for a combination of different experimental approaches in order to fully understand the dynamic organisation of cytoskeletons, from simplified *in vitro* systems to *in vivo* quantitative analysis. Our results show that, in oocytes, advection by cytoplasmic flows contributes to the polarisation of MTs by affecting the direction of growth of the plus ends.

REFERENCES

1. Mitchison, T. & Kirschner, M. Dynamic instability of microtubule growth. *Nature* **312,** 237–242 (1984).
2. Akhmanova, A. & Steinmetz, M. O. Control of microtubule organization and dynamics: two ends in the limelight. *Nat. Rev. Mol. Cell Biol.* **16,** 711–726 (2015).
3. Nieuwburg, R. *et al.* Localised dynactin protects growing microtubules to deliver *oskar* mRNA to the posterior cortex of the *Drosophila* oocyte. *eLife Sciences* **6,** e27237 (2017).
4. Purro, S. A. *et al.* Wnt Regulates Axon Behavior through Changes in Microtubule Growth Directionality: A New Role for Adenomatous Polyposis Coli. *J. Neurosci.* **28,** 8644–8654 (2008).
5. Fassier, C. *et al.* Motor axon navigation relies on Fidgetin-like 1–driven microtubule plus end dynamics. *J. Cell Biol.* **217,** 1719–1738 (2018).
6. Kent, I. A., Rane, P. S., Dickinson, R. B., Ladd, A. J. C. & Lele, T. P. Transient Pinning and Pulling: A Mechanism for Bending Microtubules. *PLoS ONE* **11,** e0151322 (2016).
7. Jiang, K. *et al.* A Proteome-wide Screen for Mammalian SxIP Motif-Containing Microtubule Plus-End Tracking Proteins. *Current Biology* **22,** 1800–1807 (2012).
8. Kodama, A., Karakesisoglou, I., Wong, E., Vaezi, A. & Fuchs, E. ACF7: An essential integrator of microtubule dynamics. *Cell* **115,** 343–354 (2003).
9. Parton, R. M. *et al.* A PAR-1-dependent orientation gradient of dynamic microtubules directs posterior cargo transport in the *Drosophila* oocyte. *The Journal of Cell Biology* **194,** 121–135 (2011).
10. Nashchekin, D., Fernandes, A. R. & St Johnston, D. Patronin/Shot Cortical Foci Assemble the Noncentrosomal Microtubule Array that Specifies the *Drosophila* Anterior-Posterior Axis. *Dev. Cell* **38,** 61–72 (2016).
11. Doerflinger, H., Benton, R., Torres, I. L., Zwart, M. F. & St Johnston, D. *Drosophila* anterior-posterior polarity requires actin-dependent PAR-1 recruitment to the oocyte posterior. *Current Biology* **16,** 1090–1095 (2006).
12. Palacios, I. M. & St Johnston, D. *Kinesin light chain*-independent function of the K*inesin heavy chain* in cytoplasmic streaming and posterior localisation in the *Drosophila* oocyte. *Development* **129,** 5473–5485 (2002).
13. Ganguly, S., Williams, L. S., Palacios, I. M. & Goldstein, R. E. Cytoplasmic streaming in *Drosophila* oocytes varies with kinesin activity and correlates with the microtubule cytoskeleton architecture. *Proc. Natl. Acad. Sci. U.S.A.* **109,** 15109–15114 (2012).
14. Hurd, T. R. *et al.* Long Oskar Controls Mitochondrial Inheritance in *Drosophila melanogaster*. *Dev. Cell* **39,** 560–571 (2016).
15. Forrest, K. M. & Gavis, E. R. Live imaging of endogenous RNA reveals a diffusion and entrapment mechanism for *nanos* mRNA localization in *Drosophila*. *Curr. Biol.* **13,** 1159–1168 (2003).

16. Lu, W. *et al.* Ooplasmic flow cooperates with transport and anchorage in *Drosophila* oocyte posterior determination. *The Journal of Cell Biology* **217,** 3497–3511 (2018).
17. Monteith, C. E. *et al.* A Mechanism for Cytoplasmic Streaming: Kinesin-Driven Alignment of Microtubules and Fast Fluid Flows. *Biophys. J.* **110,** 2053–2065 (2016).
18. Lu, W., Winding, M., Lakonishok, M., Wildonger, J. & Gelfand, V. I. Microtubule-microtubule sliding by kinesin-1 is essential for normal cytoplasmic streaming in *Drosophila* oocytes. *Proc. Natl. Acad. Sci. U.S.A.* **113,** E4995–5004 (2016).
19. Drechsler, M., Giavazzi, F., Cerbino, R. & Palacios, I. M. Active diffusion and advection in *Drosophila* oocytes result from the interplay of actin and microtubules. *Nat Comms* **8,** 1520 (2017).
20. Shimada, Y., Yonemura, S., Ohkura, H., Strutt, D. & Uemura, T. Polarized transport of Frizzled along the planar microtubule arrays in *Drosophila* wing epithelium. *Dev. Cell* **10,** 209–222 (2006).
21. Horn, B. K. P. & Schunck, B. G. Determining optical flow. *Artificial Intelligence* **17,** 185–203 (1981).
22. Vig, D. K., Hamby, A. E. & Wolgemuth, C. W. On the Quantification of Cellular Velocity Fields. *Biophys. J.* **110,** 1469–1475 (2016).
23. Ruhnau, P., Kohlberger, T., Schnörr, C. & Nobach, H. Variational optical flow estimation for particle image velocimetry. *Experiments in Fluids* **38,** 21–32 (2005).
24. Amat, F., Myers, E. W. & Keller, P. J. Fast and robust optical flow for time-lapse microscopy using super-voxels. *Bioinformatics* **29,** 373–380 (2013).
25. Boric, K., Orio, P., Viéville, T. & Whitlock, K. Quantitative analysis of cell migration using optical flow. *PLoS ONE* **8,** e69574 (2013).
26. Guo, D., van de Ven, A. L. & Zhou, X. Red blood cell tracking using optical flow methods. *IEEE J Biomed Health Inform* **18,** 991–998 (2014).
27. Lombardot, B. *et al.* Evaluation of four 3D non rigid registration methods applied to early zebrafish development sequences. *In Proceedings of the Third MICCAI Workshop on Microscopic Image Analysis with Applications in Biology* (2008).
28. Melani, C. *et al.* Cells tracking in a live zebrafish embryo. *Conf Proc IEEE Eng Med Biol Soc* **2007,** 1631–1634 (2007).
29. Pizarro, L., Delpiano, J., Aljabar, P., Ruiz-del-Solar, J. & Rueckert, D. Towards dense motion estimation in light and electron microscopy. in 1939–1942 (IEEE, 2011). doi:10.1109/ISBI.2011.5872789
30. Schmid, B. *et al.* High-speed panoramic light-sheet microscopy reveals global endodermal cell dynamics. *Nat Comms* **4,** (2013).
31. Kirisits, C., Lang, L. F. & Scherzer, O. Optical Flow on Evolving Surfaces with Space and Time Regularisation. *Journal of Mathematical Imaging and Vision* **52,** 55–70 (2015).

32. Boquet-Pujadas, A. *et al.* BioFlow: a non-invasive, image-based method to measure speed, pressure and forces inside living cells. *Scientific Reports* **7,** (2017).
33. Huang, Y., Hao, L., Li, H., Liu, Z. & Wang, P. Quantitative Analysis of Intracellular Motility Based on Optical Flow Model. *J Healthc Eng* **2017,** 1848314 (2017).
34. Delpiano, J. *et al.* Performance of optical flow techniques for motion analysis of fluorescent point signals in confocal microscopy. *Machine Vision and Application* (2012). doi:10.1007/s00138-011-0362-8
35. Frerking, L., Burger, M., Vestweber, D. & Brune, C. TGV-based flow estimation for 4D leukocyte transmigration. in 79–83 (IOP, 2014).
36. Karpova, N., Bobinnec, Y., Fouix, S., Huitorel, P. & Debec, A. Jupiter, a new *Drosophila* protein associated with microtubules. *Cell Motil. Cytoskeleton* **63,** 301–312 (2006).
37. Theurkauf, W. E. Premature Microtubule-Dependent Cytoplasmic Streaming in Cappuccino and Spire Mutant Oocytes. *Science* **265,** 2093–2096 (1994).
38. Dahlgaard, K., Raposo, A. A. S. F., Niccoli, T. & St Johnston, D. Capu and Spire assemble a cytoplasmic actin mesh that maintains microtubule organization in the *Drosophila* oocyte. *Dev. Cell* **13,** 539–553 (2007).
39. Quinlan, M. E. Direct interaction between two actin nucleators is required in *Drosophila* oogenesis. *Development* **140,** 4417–4425 (2013).
40. Rudin, L. I., Osher, S. & Fatemi, E. Nonlinear total variation based noise removal algorithms. *Physica D: Nonlinear Phenomena* **60,** 259–268 (1992).
41. Baker, S. *et al.* A Database and Evaluation Methodology for Optical Flow. *Int J Comput Vision* **92,** 1–31 (2011).
42. Gonzales-Reyes, A., Elliott, H. & St Johnston, D. Polarization of Both Major Body Axes in *Drosophila* by *Gurken-Torpedo* Signaling. *Nature* **375,** 654–658 (1995).
43. Roth, S., Shira Neuman-Silberberg, F., Barcelo, G. & Schüpbach, T. *cornichon* and the EGF receptor signaling process are necessary for both anterior-posterior and dorsal-ventral pattern formation in *Drosophila*. *Cell* **81,** 967–978 (1995).
44. Januschke, J. *et al.* Polar transport in the *Drosophila* oocyte requires Dynein and Kinesin I cooperation. *Curr. Biol.* **12,** 1971–1981 (2002).
45. Brendza, R. P., Serbus, L. R., Duffy, J. B. & Saxton, W. M. A Function for Kinesin I in the Posterior Transport of oskar mRNA and Staufen Protein. *Science* **289,** 2120–2122 (2000).
46. Brendza, K. M., Rose, D. J., Gilbert, S. P. & Saxton, W. M. Lethal kinesin mutations reveal amino acids important for ATPase activation and structural coupling. *J. Biol. Chem.* **274,** 31506–31514 (1999).
47. Loiseau, P., Davies, T., Williams, L. S., Mishima, M. & Palacios, I. M. *Drosophila* PAT1 is required for Kinesin-1 to transport cargo and to maximize its motility. *Development* **137,** 2763–2772 (2010).

48. Serbus, L. R. Dynein and the actin cytoskeleton control kinesin-driven cytoplasmic streaming in *Drosophila* oocytes. *Development* **132,** 3743–3752 (2005).
49. Zimyanin, V. L. *et al.* In vivo Imaging of *oskar* mRNA transport reveals the mechanism of posterior localization. *Cell* **134,** 843–853 (2008).
50. Williams, L. S., Ganguly, S., Loiseau, P., Ng, B. F. & Palacios, I. M. The auto-inhibitory domain and ATP-independent microtubule-binding region of Kinesin heavy chain are major functional domains for transport in the *Drosophila* germline. *Development* **141,** 176–186 (2014).
51. Tanaka, T., Kato, Y., Matsuda, K., Hanyu-Nakamura, K. & Nakamura, A. *Drosophila* Mon2 couples Oskar-induced endocytosis with actin remodeling for cortical anchorage of the germ plasm. *Development* **138,** 2523–2532 (2011).
52. Lopez, M. P. *et al.* Actin-microtubule coordination at growing microtubule ends. *Nat Comms* **5,** (2014).
53. Papenberg, N., Bruhn, A., Brox, T., Didas, S. & Weickert, J. Highly Accurate Optic Flow Computation with Theoretically Justified Warping. *Int J Comput Vision* **67,** 141–158 (2006).
54. Quinlan, M. E. Cytoplasmic Streaming in the *Drosophila* Oocyte. *Annu. Rev. Cell Dev. Biol.* **32,** 173–195 (2016).
55. Fakhri, N. *et al.* High-resolution mapping of intracellular fluctuations using carbon nanotubes. *Science* **344,** 1031–1035 (2014).
56. Katrukha, E. A. *et al.* Probing cytoskeletal modulation of passive and active intracellular dynamics using nanobody-functionalized quantum dots. *Nat Comms* **8,** 14772 (2017).
57. Brangwynne, C. P., MacKintosh, F. C. & Weitz, D. A. Force fluctuations and polymerization dynamics of intracellular microtubules. *Proc. Natl. Acad. Sci. U.S.A.* **104,** 16128–16133 (2007).
58. Brangwynne, C. P. *et al.* Microtubules can bear enhanced compressive loads in living cells because of lateral reinforcement. *J. Cell Biol.* **173,** 733–741 (2006).
59. Khuc Trong, P., Doerflinger, H., Dunkel, J., St Johnston, D. & Goldstein, R. E. Cortical microtubule nucleation can organise the cytoskeleton of *Drosophila* oocytes to define the anteroposterior axis. *eLife Sciences* **4,** 4155 (2015).
60. Brendza, R. P., Serbus, L. R., Saxton, W. M. & Duffy, J. B. Posterior localization of dynein and dorsal-ventral axis formation depend on kinesin in *Drosophila* oocytes. *Curr. Biol.* **12,** 1541–1545 (2002).
61. Moua, P., Fullerton, D., Serbus, L. R., Warrior, R. & Saxton, W. M. Kinesin-1 tail autoregulation and microtubule-binding regions function in saltatory transport but not ooplasmic streaming. *Development* **138,** 1087–1092 (2011).
62. Cai, D., McEwen, D. P., Martens, J. R., Meyhofer, E. & Verhey, K. J. Single Molecule Imaging Reveals Differences in Microtubule Track Selection Between Kinesin Motors. *PLOS Biology* **7,** e1000216 (2009).

63. Wang, Y. & Riechmann, V. Microtubule anchoring by cortical actin bundles prevents streaming of the oocyte cytoplasm. *Mech. Dev.* **125,** 142–152 (2008).

64. Chou, T. B. & Perrimon, N. The autosomal FLP-DFS technique for generating germline mosaics in *Drosophila melanogaster*. *Genetics* **144,** 1673–1679 (1996).

65. Schindelin, J. *et al.* Fiji: an open-source platform for biological-image analysis. *Nature Methods* **9,** 676–682 (2012).

66. Chambolle, A. & Pock, T. A First-Order Primal-Dual Algorithm for Convex Problems with Applications to Imaging. *Journal of Mathematical Imaging and Vision* **40,** 120–145 (2011).

ACKNOWLEDGEMENTS

We thank Dr D. St Johnston and I. Davis for reagents, and M. Wayland for assistance with imaging. We also thank Lena Frerking and Sujoy Ganguly for fruitful discussions during the initial phase of the project. MD and IMP were supported by the BBSRC, the University of Cambridge and Queen Mary University of London. MD was also supported by an Isaac Newton Trust fellowship and acknowledges funding by the DFG/SFB944 ('Physiology and Dynamics of Cellular Microcompartments'). LFL and CBS acknowledge support from the Leverhulme Trust ('Breaking the non-convexity barrier'), EPSRC (grant No. EP/M00483X/1), the EPSRC Centre (No. EP/N014588/1), the RISE projects CHiPS and NoMADS, the Cantab Capital Institute for the Mathematics of Information, and the Alan Turing Institute. MB und HD acknowledge support by the European Research Council (EU FP7-ERC Consolidator Grant No. 615216 LifeInverse). We gratefully acknowledge the support of NVIDIA Corporation with the donation of the Quadro P6000 GPU used for this research.

AUTHOR CONTRIBUTIONS

MD designed and performed experiments, analysed the data, discussed results and wrote the manuscript. IMP designed experiments, analysed the data, discussed results and wrote the manuscript. LFL and CBS developed the code required for the OF image analysis, analysed the data, discussed the results, and wrote the manuscript. HD developed code for the OF image analysis. MB contributed to the discussion and ideas during the initial implementation phase of the project.

COMPETING INTERESTS

The authors declare no competing financial interests.

DATA AVAILABILITY

The source code of our implementation and of the data analysis is available online (https://doi.org/10.5281/zenodo.2573254). All relevant data and the computational results are available from the corresponding authors upon request.

METHODS

Fly stocks and genetics

Flies were kept at standard corn meal agar and raised at room temperature (21°C). Detailed genotypes of all fly stocks can be found in Supplementary Table 1. Homozygous *capu* mutant flies were viable. Germ line clones for the analysis of *khc* mutant alleles have been induced by the FLP/FRT ovoD system[64]. Germline clones in Figure 5 were identified by the absence of nuclear GFP in germline cells.

Live imaging

Female flies of the desired genotypes were collected and fattened on dry yeast for 12-16 h prior to imaging. Ovaries were dissected in a small drop of halocarbon oil (Voltalef S10, VWR) on a glass coverslip and single egg chambers were separated using fine tungsten needles. Images were acquired on a Leica SP5 inverted confocal microscope, using a 40×/1.3 Oil DIC Plan-Neofluar (Jup) or a 100×/1.4 Oil DIC objective (EB1). Signals were detected using a Leica HyD Hybrid Detector. For MT bulk movement, a single plane from the middle of the oocyte was imaged at a scan speed of 100 Hz and at an image resolution of 1,024 × 1,024 pixels (corresponding to one image every 10.4 s). For EB1 imaging the oocyte was fitted and oriented within a 512 x 256 pixels frame and a single plane image was taken every 0.65 s. Image sequences of at least 100 frames (65 s) were taken, inspected visually, and bleach corrected using Fiji[65].

Immunostainings

Egg chambers were dissected in PBS+0.1% Tween20 and fixed in 10% formaldehyde in PBS+0.1% Tween20 for 10 min. Fixed ovaries were incubated with an anti-αTubulin primary antibody (MAB1864, Sigma-Aldrich, cloneYL1/2), diluted 1:100 in PBS+2% Tween20 over night at 4˚. After four consecutive washes Alexa568-coupled secondary antibodies (1:100) were incubated were incubated for two hour at room temperature. Native fluorescence of GFP was imaged without amplification. Images were acquired on a Leica SP5 inverted confocal microscope, using a 40×/1.3 Oil DIC Plan-Neofluar objective.

Image denoising and optical flow (OF)-based motion estimation

Motion analysis of the recorded two-dimensional image sequences was performed using a two-step procedure. The first step aimed to remove noise contamination from the unprocessed sequences, while the goal of the second step was to estimate displacement vector fields from the improved sequences. In the first step, we recovered from each noisy (grey-valued) image sequence u^δ an improved version u by solving a variational image denoising problem with spatio-temporal regularisation. It reads

$$u = \operatorname{argmin}_u \frac{1}{2}\left\|u - u^\delta\right\|^2 + \alpha_1 \|\nabla u\|_{2,1} + \frac{\beta_1}{2}\|\partial_t u\|^2.$$

While the first two terms on the right-hand side resemble standard image denoising with total variation regularisation[40] in space, the third term connects subsequent frames by penalising temporal changes in the recovered solution. As EB1 comets typically appear in several subsequent frames at similar positions, it allows to effectively remove randomly distributed noise from a sequence (see Figure 2d,e, Supplementary Movie 2, and Supplementary Methods). Here, $\alpha, \beta > 0$ are regularisation parameters that balance the three terms and need to be chosen appropriately. Moreover, the norms are taken over the entire image sequence.

The result u served as input to the motion estimation step, in which we estimated a displacement vector field v by solving

$$v = \operatorname{argmin}_v \frac{1}{2} \|\partial_t u + \langle \nabla u, v \rangle\|^2 + \alpha_2 \|\nabla v\|_{2,1} + \frac{\beta_2}{2} \|\partial_t v\|_{2,2}^2.$$

Here, the first term on the right-hand side aims to approximately solve the optical flow equation[21], while the second and third terms incorporate spatio-temporal regularisation of the vector-valued unknown (for a derivation of the model and further details see Supplementary Methods). The use of the vector-valued total variation allows for spatial discontinuities in the displacement vector field. We found that in both steps the temporal regularisation was key and the analysis of individual frames did not yield satisfactory results.

Both finite-dimensional minimisation problems were approximately solved using the primal-dual hybrid gradient method[66] and graphics-processing unit (GPU) acceleration. An in-depth description of both models, their numerical solution, and parameter choices as well as implementation details can be found in the Supplementary Methods.

716 **FIGURE LEGENDS**

Figure 1 - Drechsler and Lang et al.

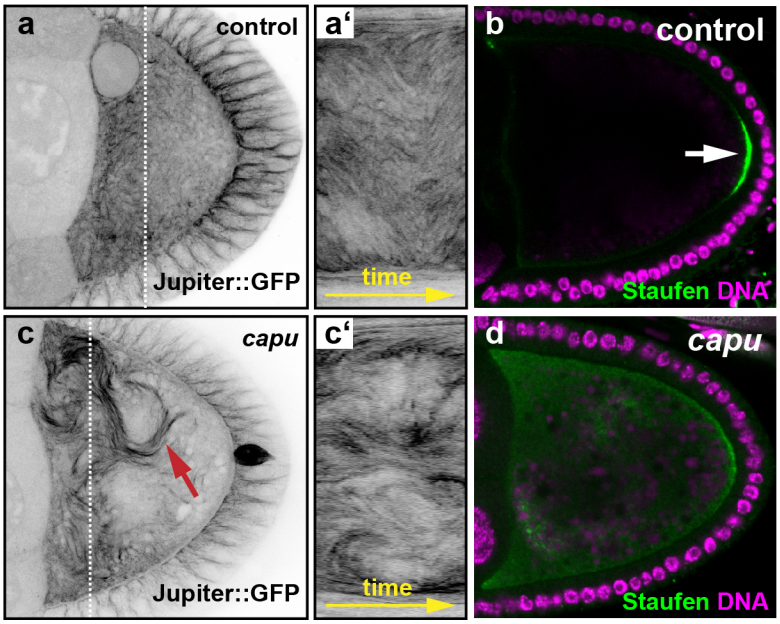

717

718 **Figure 1 – MT bulk movement in control and *capu* mutant oocytes and posterior cargo**
719 **distribution. a)** Living control oocyte, expressing the MT-binding protein Jup (Supplementary Movie
720 1). **a')** Kymograph/space-time plot (along the indicated dotted line in a), showing dynamic bending
721 of MTs over time. **b)** Staufen (green) localisation in control. The protein localises in a tight posterior
722 crescent by the end of st9. **c)** Living *capu* mutant oocyte, expressing Jup. Fast cytoplasmic flows,
723 induced by the lack of the actin nucleator Cappuccino (*capu*), lead to the formation of dense and
724 long MT bundles (red arrow), as well as an increased bending of MTs in the oocyte (Supplementary
725 Movie 1). **c')** Kymograph (along dashed line in b) also indicates a stronger displacement of bundled
726 MTs over time in *capu* mutants. **d)** Staufen fails to localise in *capu* mutants and distributed
727 throughout the cytoplasm of the cell.

728
729
730
731
732
733
734
735
736
737
738
739
740
741

Figure 2 - Drechsler and Lang et al.

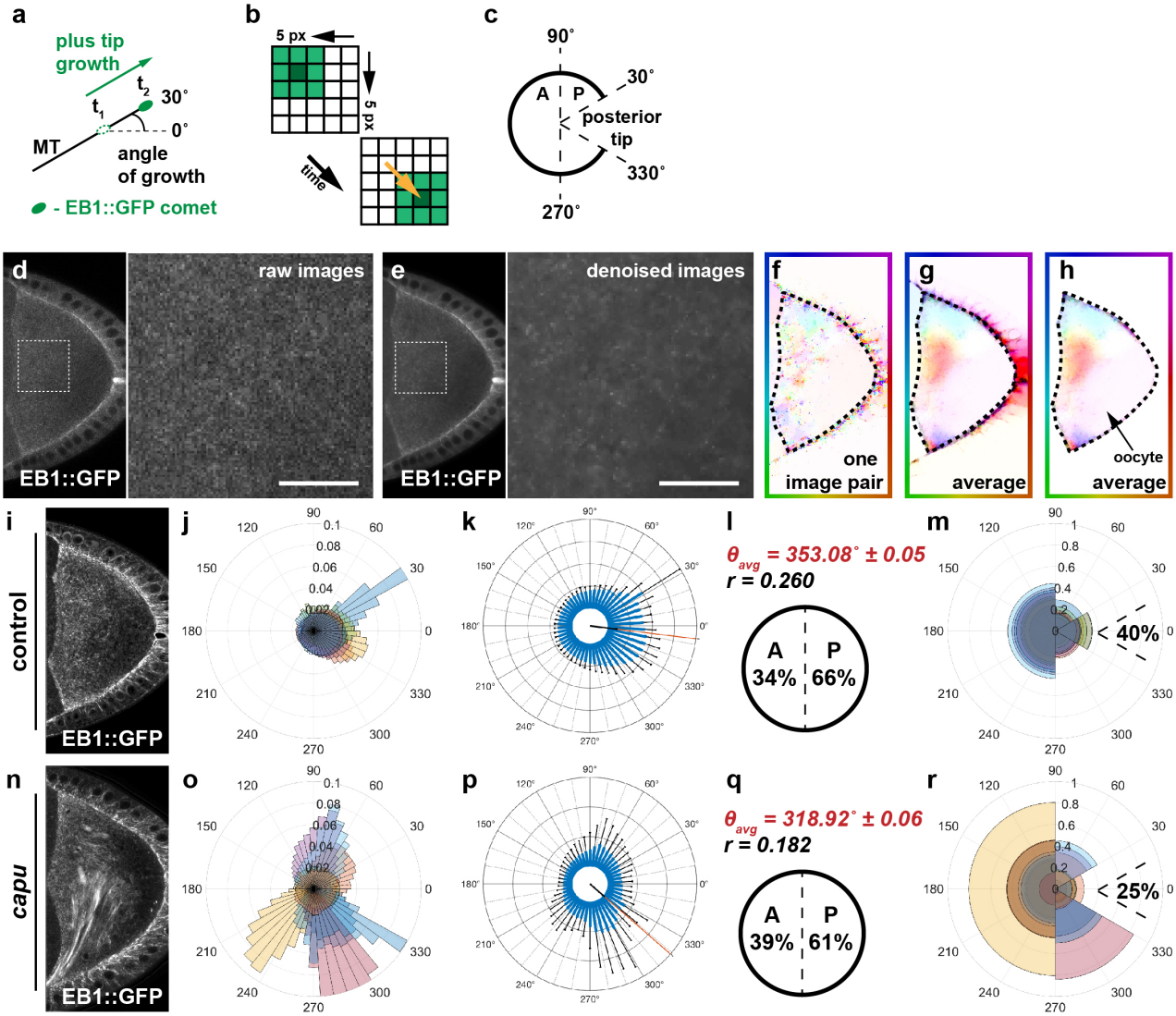

742

743 **Figure 2 – Optical flow analysis captures MT orientation in control and *capu* mutant oocytes.**
744 **a)** Schematic representation of MT orientation. EB1 specifically associates with the growing end
745 (plus-end) of MTs and therefore serves as read out of their spatial orientation. The orientation of MT
746 growth is represented as angle, deviating from an imaginary anterior (180°) to posterior axis (0°). **b)**
747 Simplified scheme that illustrates the underlying principle of OF-based motion estimation. Shown
748 are two consecutive frames of size 5 x 5 pixels of a synthetic image sequence that contains a
749 rectangular object of different pixel intensities - from light green (little signal) to dark green (maximum
750 signal). For better visibility an inverted colour scheme is used, as EB1 comets typically appear as
751 bright spots. OF assumes that the intensities of a signal do not change along its trajectory. Based
752 on this assumption, variational OF allows to estimate a displacement vector for each pixel (the yellow
753 arrow shows the displacement vector of the centre pixel of the object). **c)** Definition of growth
754 direction based on OF-estimated velocities. Angles of velocities between 90°-270° are regarded as
755 anterior (A), the complementary set of angles as posterior (P). Angles within the pool of posterior-
756 growing comets that fall between 330°-30° are considered to grow towards the posterior tip. **d)** Single
757 frame of an unprocessed image sequence (raw data) showing an oocyte expressing EB1. The
758 magnified area is indicated by a dashed box. **e)** Same frame as shown in (d), after applying the

denoising step (Supplementary Movie 2). Scale bars are 10 µm. **f)** Shown is the optical flow (displacement vector field) between two frames of the image sequence in (a). **g)** Average optical flow (over all pairs of frames of the sequence). **h)** Hand-drawn segmentation mask of the oocyte. For the analysis, only the displacement vectors within this segmentation were considered. **i)** Standard deviation projection of EB1 comets in a control image sequence (in total 650 s). **j)** Rose diagram (angular histogram) with 50 bins depicting the distribution of EB1 growth directions in individual control cells within the corresponding segmented oocyte. Each colour represents the angular histogram of the directions from one oocyte. **k)** Same data as shown in (j) with angular histograms averaged over all cells (n=8). Error bars (in black) indicate the standard deviation for each bin (in blue). **l)** Mean angular direction θ_{avg} of the histogram shown in (k) (also indicated by a red line in (k)) and the length r (between 0 and 1) of the mean resultant vector (length of black line in (k) originating from the centre), which relates to the circular variance $S = 1 - r$ of the distribution shown in (k). Anterior-posterior bias of all EB1 growth directions. **m**) Rose diagram similar to (j) for control cells but with growth directions binned into four bins (30°-90°, 90°-270°, 270°-330°, and 330°-30°). Moreover, the fraction of posterior-growing EB1 comets pointing towards the posterior tip (330°-30°) is indicated. **n-r)** Same representation as in (i)-(m) but for the estimated EB1 growth directions of *capu* mutant oocytes (n=10).

Figure 3 - Drechsler and Lang et al.

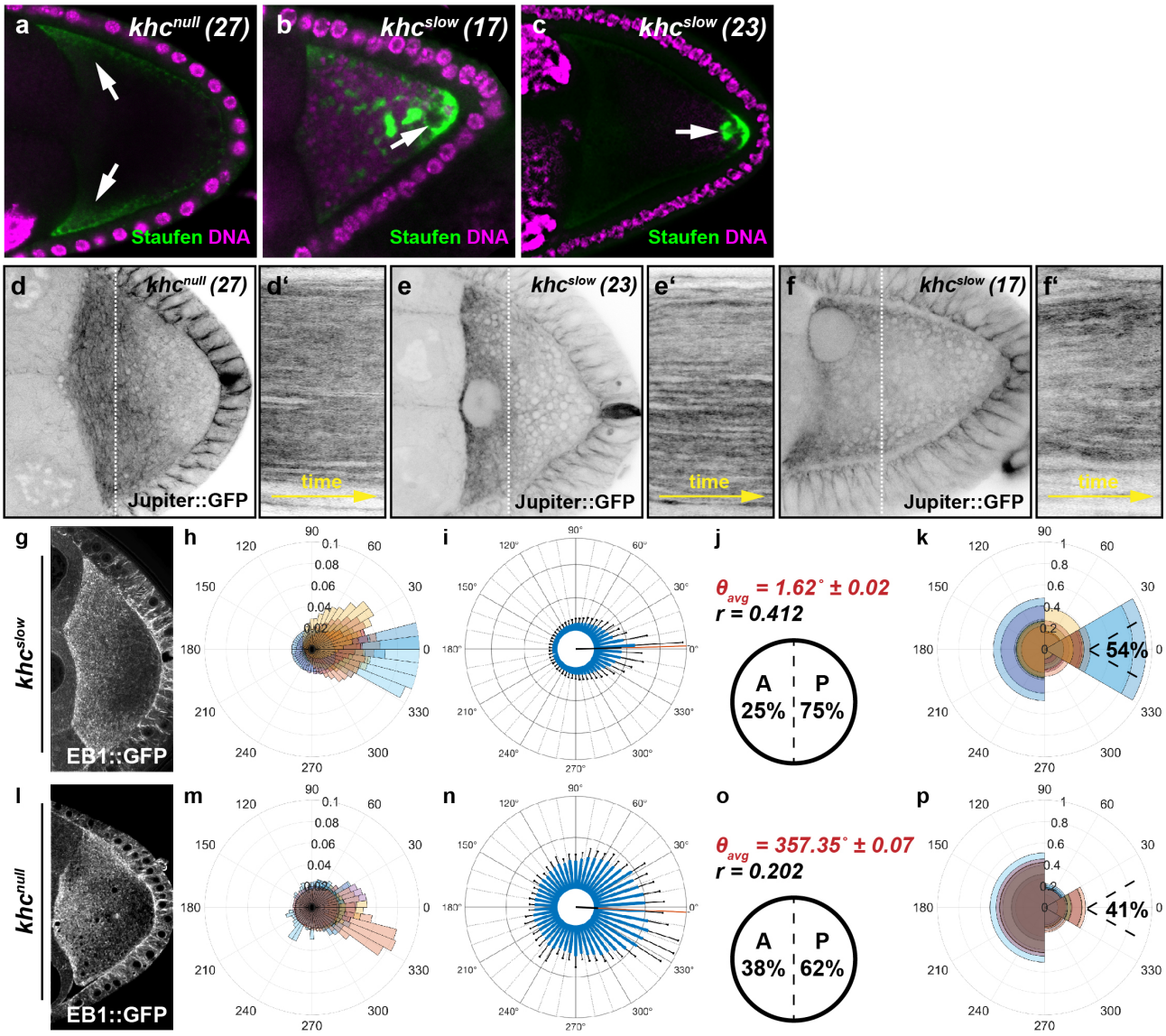

Figure 3 – Kin activity impacts on the spatial orientation of MTs in the oocyte. a-c) Posterior cargo localisation in different *khc* mutant alleles. Staufen (green) is not transported in cells lacking Kin (*khc*^{null} *(27)*) and is found in the anterior corners of the cell (arrows). In contrast, in both of the slow Kin alleles (*khc*^{slow} *(23)* and *khc*^{slow} *(17)*) a considerable amount of Staufen becomes transported towards posterior. However, compared to controls (Figure 1b) Staufen does not localise in a tight posterior crescent but rather in dots within the posterior cytoplasm (arrows). **d-f)** Still frames and kymographs of live oocytes expressing Jup. Cells harbour a null mutation (*khc*^{null} *(27)*), or single point mutations (*khc*^{slow} *(23)* and *khc*^{slow} *(17)*) in the motor domain, rendering the motor slower. Compared to controls, all *khc* mutant cells exhibit no cytoplasmic flows and thus no MT bulk motion (Supplementary Movie 6). **g-p)** OF analysis of EB1 growth directionality in *khc*^{sllow} (g-k, n=10) and *khc*^{null} (l-p, n=10) oocytes.

Figure 4 - Drechsler and Lang et al.

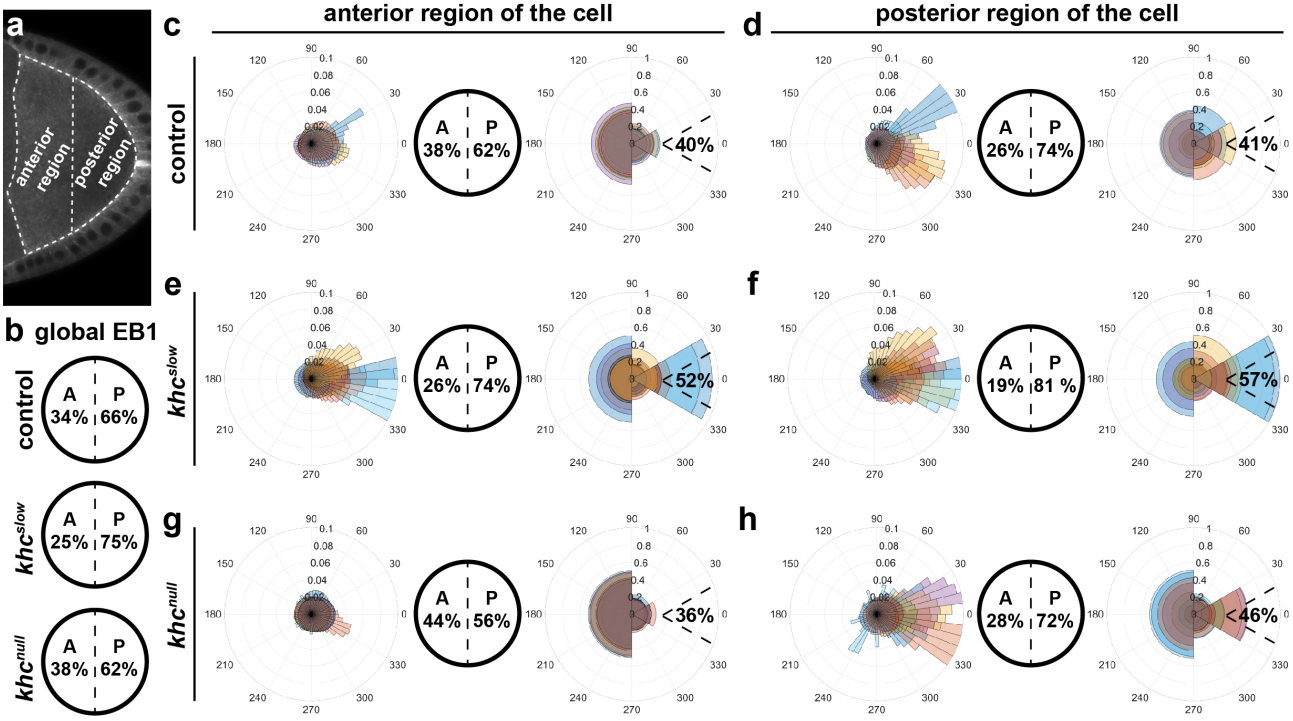

Figure 4 – Regional impact of Kin activity on MT orientation. a) Single frame of an oocyte expressing EB1. Dashed lines represent the anterior and posterior regions of the oocyte used to extract orientation data. **b)** Global EB1 signal directions within the entire oocyte (as shown in Figures 2 and 3). **c-h)** In each case, from left to right: distribution of EB1 growth orientation in the indicated region of the cells visualised in a rose diagram, the anterior-posterior orientation, and the posterior tip orientation. **c,d)** Data for control cells (n=8). **e,f)** Data for *khc*^{slow} mutant cells (n=10). **g,h)** Data for *khc*^{null} mutant cells (n=10).

Figure 5 - Drechsler and Lang et al.

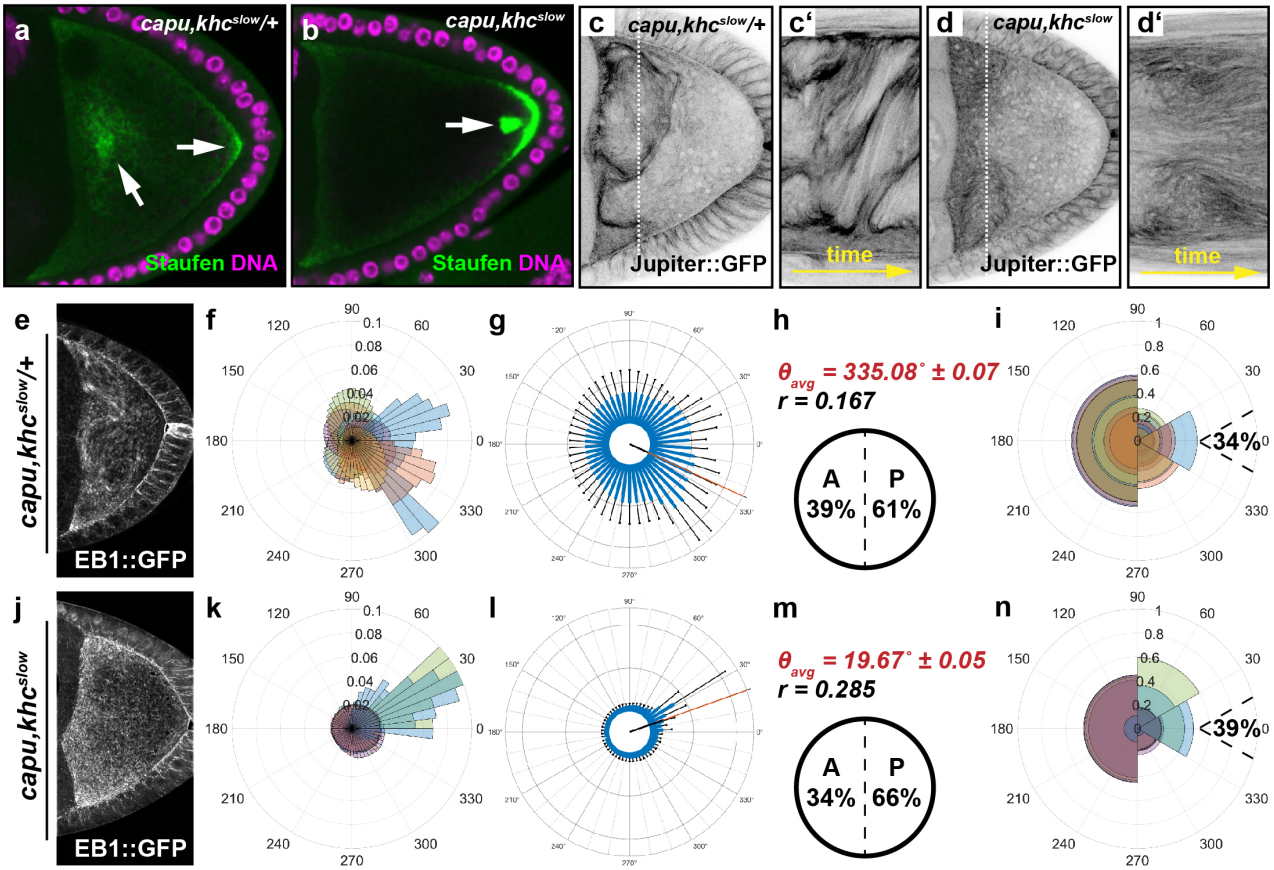

Figure 5 – Cytoplasmic flows constitute a major contributor to MT orientation. a,b) Posterior cargo localisation in *capu,khc^{slow}/+ and capu,khc^{slow}* double mutant cells. In *capu,khc^{slow}/+* oocytes, the majority of Staufen protein (green) localises as a cytoplasmic cloud (a). In *capu,khc^{slow}* double mutant cells, Staufen localises in a posterior crescent but also accumulates in dots close to the posterior. **c,d)** Still frames and kymographs of live *capu,khc^{slow}/+* (c,c') or *capu,khc^{slow}* double mutant oocytes (d,d'), expressing Jup. **e-n)** OF analysis of EB1 growth directionality in *capu,khc^{slow}/+* (e-i, n=10) and *capu,khc^{slow}* (j-n, n=8) oocytes.

Figure 6 - Drechsler and Lang et al.

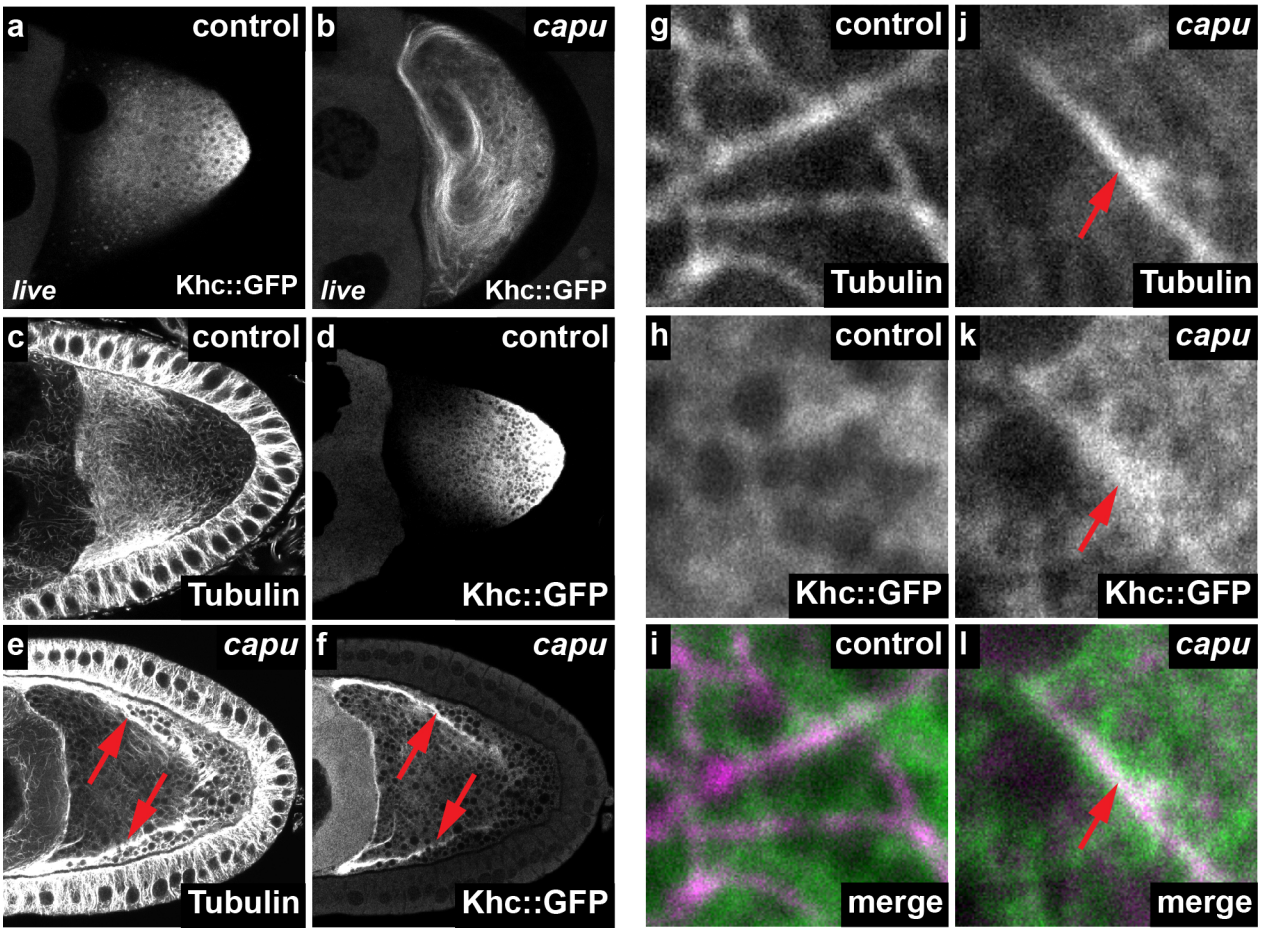

Figure 6 – A potential link between the actin mesh and Kin recruitment to MTs. a,b) Living control (a) and *capu* mutant oocyte (b), expressing Khc1-700::GFP. While the fusion protein mainly localises posteriorly in control cells (a), it strongly decorates MTs in *capu* mutant cells (b and Supplementary Movie 10). **c-f)** Fixed control oocytes (c,d) and *capu* mutants (e,f), expressing Khc::GFP. Cells were stained against αTubulin and the GFP fusion protein. In controls, Tubulin and Khc1-700::GFP localise to opposed gradients and show little or no overlap (c,d). Conversely, in *capu* mutants, Khc::GFP strongly co-localises to areas with high Tubulin intensity (red arrows in e,f). **g-l)** High resolution images of fixed control (g-i) and *capu* mutant (j-l) cells, stained against αTubulin (magenta) and GFP (green). While KHC::GFP localises diffusely around MTs in control cells (g-i), it strongly co-localises to MTs in *capu* mutants (red arrows in j-l)

Table 1 – Summary of EB1 orientation data, extracted from confocal time series by variational OF analysis.

		global EB1::GFP					EB1::GFP in anterior oocyte			EB1::GFP in posterior oocyte		
genotype	***n***	**% ant.**	**% post.**	**% post. tip**	θ_{avg}	***r***	**% ant.**	**% post.**	**% post. tip**	**% ant.**	**% post.**	**% post. tip**
control	8	34 ± 6	66 ± 6	40 ± 4	353.08±0.05	0.260	38 ± 5	62 ± 5	40 ± 5	26 ± 11	74 ± 11	41 ± 8
grk	3	28 ± 72	72 ± 72	41 ± 44	329.65±0.07	0.339						
capu	10	39 ± 14	61 ± 14	25 ± 8	318.92±0.06	0.182						
khc^{null}	10	38 ± 6	62 ± 6	41 ± 7	357.35±0.07	0.202	44 ± 4	56 ± 4	36 ± 3	28 ± 13	72 ± 13	46 ± 13
khc^{slow}	10	25 ± 10	75 ± 10	54 ± 15	1.62±0.02	0.412	26 ± 11	74 ± 11	52 ± 14	19 ± 10	81 ± 10	57 ± 17
capu,khc^{slow}\+	10	39 ± 13	61 ± 13	34 ± 5	335.08±0.07	0.167						
capu,khc^{slow}	8	34 ± 15	66 ± 15	39 ± 5	19.67±0.05	0.285						
Tracking data from Parton et al. 2011												
control		42	58				46	54		37	63	
par-1		49	51									

similar to control
stronger posterior bias
weaker posterior bias

Anterior-posterior orientation bias of microtubule growth in per cent (± 95% confidence interval). *n* represents the number of cells analysed. θ_{avg} gives the average angle of all EB1 orientations of all cells of a given genotype. *r* constitutes a measure of variance and lies between 0 and 1. The larger *r*, the less variable the data set.

878